Advances in Adaptive Data Analysis
Vol. 1, No. 1 (2009) 89–123

World Scientific
www.worldscientific.com

A RECORDING-BASED APPROACH FOR IDENTIFYING SEISMIC SITE LIQUEFACTION AND NONLINEARITY VIA HHT DATA ANALYSIS

RAY RUICHONG ZHANG

Division of Engineering, Colorado School of Mines
Golden, CO 80401, USA

This study proposes an approach to identify earthquake-induced site liquefaction and/or nonlinearity from Hilbert–Huang–Transformation- or HHT-based data analysis of seismic motion recordings. The proposed approach fully utilizes unique features of the HHT method in characterizing instantaneous frequency and damping as well as temporal-frequency motion from the recordings, so as to single out and quantify liquefaction- and/or nonlinear-soil-related nonlinear phenomena shown in the recordings. With post-earthquake, site investigation as a reference, this study shows that the proposed approach is effective in characterizing site nonlinearity, quantifying nonlinear influences in site amplification, and diagnosing site liquefaction. Major results from this study are listed below.

1. Predominant instantaneous frequency of earthquake motion is defined as the frequency with the largest amplitude in Hilbert amplitude spectra of the motion at a time instant, and subsequently used together with other motion features for identifying site liquefaction conditions. Analysis of 29 sets of seismic recordings with different liquefaction conditions shows that the proposed approach is more effective in detecting site liquefaction than other Fourier-based methods.
2. HHT-based site amplification is defined as the ratio of marginal Hilbert amplitude spectra, similar to the Fourier-based one that is the ratio of Fourier amplitude spectra. The HHT-based site amplification can be used for effectively quantifying site nonlinearity in terms of frequency downshift in the low-frequency range and amplification-reduction factor in intermediate-frequency range in comparison with the Fourier-based one.
3. Instantaneous damping, and Hilbert and marginal Hilbert damping spectra are defined in way similar to instantaneous frequency, and Hilbert and marginal Hilbert amplitude spectra, respectively. Consequently, the HHT-based site damping is found as the difference of marginal Hilbert damping spectra, which can be used as an alternative, complementary index to measure influences of site nonlinearity in seismic ground responses.

Keywords: Site nonlinearity; site amplification; site damping; liquefaction; Hilbert–Huang transform (HHT); Fourier transformation.

1. Introduction

Seismic damage to geotechnical and structural engineering systems (GSES) takes the form of liquefaction, partial loss of load capacity in soil, etc. Characterizing and

quantifying the aforementioned seismic damage plays an important role in, among others, mapping seismic hazards in urban areas, designing cost-effective anti-seismic GSES at different geological sites, and monitoring GSES health and diagnosing damage (e.g., Refs. 1 and 2), which can ultimately aid in effective seismic-hazard mitigation.

Site amplification is a major factor influencing the extent of seismic damage to GSES, which is not linearly proportional to the intensity of the seismic excitation at bedrock because of soil nonlinearity. Site liquefaction shows similar nonlinear phenomena in soil layer. Therefore, properly characterizing seismic damage in terms of soil nonlinearity such as stiffness reduction, damping increase, and reduction of dynamic-amplification factor with those of the linearity as a reference will help assess nonlinear influences to seismic damage potential, quantify seismic nonlinearity damage, improve seismic codes and guidance, etc.

On the other hand, recent evolution of emerging advanced technologies in data acquisition (e.g., remote, wireless sensory systems for seismic monitoring) makes it viable and robust for seismic damage diagnosis and seismic hazard assessment. Pertinent research (e.g., Ref. 3) suggests that acquisition of sensor information is not a crucial issue. Rather, the crucial algorithmic developments are needed to process the vast wealth of information and provide useful and simple measures of seismic damage.

To this end, research and development on cost-effective seismic damage evaluation in general, and earthquake-induced nonlinearity quantification in particular, becomes more and more important, which can greatly aid in efficient seismic hazard mapping and subsequently effective seismic hazard mitigation.

Currently, recording-based approach is one of the most efficient methods for characterizing and quantifying seismic damage in terms of site or structural nonlinearity. That is, a distributed set of motion sensors (e.g., accelerometers) record vibration/wave motion, which may be connected through a data acquisition system or wireless and transmitted to a central processing unit. Data processing and analysis can identify dynamic characteristics of a site or structure (usually natural frequencies and mode shapes) that are a function of physical parameters (e.g., stiffness distributions). Therefore, changes in physical properties resulting from damage may be inferred from changes in the identified dynamic characteristics using suitable algorithms.

While there exist many algorithms for identifying the aforementioned dynamic characteristics (e.g., spectral analysis, neural network, ARMA approach), the most traditional, likely most powerful, way is to employ Fourier spectral analysis (FSA) of nonstationary recordings for nonlinearity characterization. Fourier amplitude spectrum defines harmonic components globally and thus yields average characteristics over the entire duration of the data. While use of short-time or windowed Fourier transform in FSA may possibly minimize nonstationarity in the recordings rooted primarily in excitation, it also reduces frequency resolution as the length of the data window shortens. Thus, one is faced with a trade-off. The shorter the window, the better the temporal localization of the Fourier amplitude spectrum, but the poorer

the frequency resolution, which directly influences such measurement as downshift of modal frequencies in a low-to-intermediate frequency band. More important, FSA cannot resolve the issues of nonstationarity rooted in the system nonlinearity or nonlinear responses, which is clarified by Huang *et al.*,[4] Worden and Tomlinson,[5] Zhang *et al.*,[6] among others. Because of that, large-extent damage or nonlinearity is often distortedly identified with the FSA approach (e.g., Zhang *et al.*[7]).

Since the nonlinearity shown in seismic recordings is time-dependent, i.e., dependent upon the instantaneous amplitude of the excitation, all the dynamic parameters such as modal frequency, damping, and their changes are of temporal variation. Therefore, effectiveness of a recording-based approach for diagnosing nonlinearity damage relies on appropriateness and accuracy of temporal nonlinearity characterization from data analysis of nonstationary recordings.

The objective of this study is to propose and validate a simple, yet effective, recording-based approach, with the aid of an appropriate time-frequency data analysis similar to FSA, for quantifying nonlinearity at a site. Together with other traditional motion features, the proposed approach can be used to evaluate such seismic damage to GSES as site liquefaction and partial loss of load capacity in soil.

2. Time-Frequency Data Analysis

Alternative to the FSA approach, a method for nonstationary data processing,[4] referred to as Hilbert–Huang transform (HHT), can be used to depict seismic-induced nonlinear features from nonstationary earthquake recordings.

The HHT method consists of Empirical Mode Decomposition (EMD) and Hilbert Spectral Analysis (HSA). Any complicated time domain record can be decomposed via EMD into a finite, often small, number of intrinsic mode functions (IMF) that admit a well-behaved Hilbert transform. The IMF is defined by the following conditions: (1) over the entire time series, the number of extrema and the number of zero-crossings must be equal or differ at most by one, and (2) the mean value of the envelope defined by the local maxima and the envelope defined by the local minima is zero at any point. An IMF represents a simple oscillatory mode similar to a sinusoidal component in FSA, but more general.

The EMD explores temporal variation in the characteristic time scale of the data and thus is adaptive to nonstationary data processes. The HSA defines an instantaneous or time-dependent frequency of the data via Hilbert transformation of each IMF component. Huang *et al.*,[8] further validate the confidence limits of these two unique features. All the above, together with the recent development in instantaneous damping characterization,[6] makes the HHT method more robust and reliable in analysis of nonstationary data and revealing an enhanced interpretive value, alternative to Fourier components and amplitude spectrum.

The HHT representation of earthquake ground acceleration recording $X(t)$ is

$$X(t) = \Re \sum_{j=1}^{n} a_j(t) e^{i\theta_j(t)} = \Re \sum_{j=1}^{n} [C_j(t) + iY_j(t)], \tag{1}$$

where $C_j(t)$ and $Y_j(t)$ are, respectively the jth IMF component of $X(t)$ and its Hilbert transform $Y_j(t) = \frac{1}{\pi} P \int \frac{C_j(t')}{t-t'} dt'$ with P denoting the Cauchy principal value, and the time-dependent amplitudes $a_j(t)$ and phases $\theta_j(t)$ are the polar-coordinate expression of Cartesian-coordinate expression of $C_j(t)$ and $Y_j(t)$, from which the instantaneous frequency is defined as $\omega_j(t) = d\theta_j(t)/dt$. The Hilbert amplitude spectrum $H(\omega, t)$ and marginal Hilbert amplitude spectrum $h(\omega)$ over time duration T of the data are defined as

$$H(\omega, t) = \sum_{j=1}^{n} a_j(t), \tag{2}$$

$$h(\omega) = \int_0^T H(\omega, t) dt, \tag{3}$$

while the Hilbert and marginal Hilbert amplitude spectra provide information similar to the Fourier amplitude spectrum obtained from short-time Fourier transform, its frequency term is different. Fourier-based frequency is constant over the harmonic function persisting through the data window, while HHT-based frequency varies with time. As the Fourier transformation window length reduces to zero, the Fourier-based frequency approaches the HHT-based frequency. Fourier-based frequency is, however, locally averaged and not truly instantaneous for it depends on the window length.

3. Liquefaction Diagnosis

3.1. *Background*

Liquefaction is the phenomena of seismic generation of large pore-water pressures and consequent softening of granular soils (e.g., Kramer[9]; Youd *et al.*[10]). Reconnaissance reports on seismic hazards (e.g., Youd *et al.*[11]; Uzarski and Arnold[12]) show that liquefaction is one of the key sources responsible to the seismic damage of GSES. Therefore, identifying site liquefaction condition plays an important role in mapping seismic hazards.

One of the cost-effective approaches for detecting liquefaction is based on time-frequency analysis of ground motion recording at a site. Since the temporal variation of dynamic features (e.g., dominant frequency to be elaborated) in the seismic response/recording at a site with liquefaction differs from that without liquefaction, the temporal change of the dynamic features in ground acceleration recordings can be used as a major index, together with others (e.g., peak ground motion), to efficiently identify the status of site liquefaction, i.e., liquefaction, liquefaction suspicion, or non-liquefaction.

In particular, an earthquake ground acceleration recording at a site without liquefaction can be divided approximately into three temporal portions based on major characteristics of propagating seismic waves. The first portion of the recording shows dominant P-wave signals with high frequencies, followed by the second

portion with dominant S-wave signals at intermediate frequencies, and finally by the last part with surface and coda waves at low frequencies. Note that the aforementioned dominant waves indicate that the waves have higher amplitudes than other waves. Therefore, the corresponding dominant frequency in the recording reduces as time goes on.

With the liquefaction that usually develops at the junction of the first and second portions of the recording, soil grain skeleton at the site tends to be intensified, resulting in sharp increase of pore water pressure. The increased pore water pressure is typically not dissipated immediately during the short duration of an earthquake, leading to the reduction of effective stresses in saturated soil. Consequently the soil is in a liquefied state, partially or completely losing the loading-resistant strength. Since horizontal ground motion is attributed primarily from propagating SH and surface (e.g., Love) waves and S waves cannot propagate in the water, the dominant frequency in the horizontal-component recordings after the onset of liquefaction is typically much lower than that without liquefaction. On the other hand, because water is uncompressible and can carry P-waves, the dominant frequency of vertical-component recording with liquefaction, attributed mainly from propagating P-SV and surface (e.g., Rayleigh) waves, has a reduction after the onset of liquefaction which is similar to that without liquefaction.

The above analysis suggests that horizontal-component recordings with liquefaction will show significant drop of dominant frequency after onset of the liquefaction, which is larger than those without liquefaction. In contrast, vertical-component recording at the same site would show the reduction of dominant frequency in a comparable value as that without liquefaction.

It is of interest to note that soil nonlinearity at a non-liquefaction site results in similar phenomena in recordings as site liquefaction. They are however different in that the former typically shows great reduction of dominant frequency in three-component recordings after the onset of the site nonlinearity, while the latter only depicts significant drop in the horizontal-component recordings but not the vertical one after the onset of liquefaction.

Based on the above unique liquefaction features shown in recordings and pertinent studies in liquefaction detection (e.g., Suzuki *et al.*[13]), Kostadinov and Yamazaki[14] proposed a recording-based approach to identify site liquefaction condition, in which a key parameter associated with the aforementioned dominant frequency is the mean instantaneous frequency defined on the basis of short-time Fourier transform of the recording.

In addition, since the recordings with soil nonlinearity at a non-liquefaction site shares similar dynamic features as those with liquefaction, the aforementioned liquefaction-diagnosis approach can in principle be used for efficiently quantifying site nonlinearity, the latter of which is typically carried out with the use of two pairs of mainshock and aftershock recordings at a soil site under investigation and a reference site, respectively. This point will be elaborated later.

It is known that recordings at a liquefaction site are nonlinear responses of seismic waves propagating in the liquefied layers underneath the site. Moreover, FSA with either regular or short-time Fourier transform, distorts such dynamic features as the dominant frequency of recordings rooted in nonlinear site responses (e.g., Refs. 6 and 7). Therefore, the aforementioned Fourier-based approach is not intrinsically effective in detecting liquefaction and quantifying soil nonlinearity at a non-liquefaction site.

3.2. *HHT-based characterization and algorithm*

To characterize the dominant motion and its features from the recording, the following predominant instantaneous frequency (PIF) is defined:

$$\tilde{\omega}(t) = \hat{\omega}|_{H(\hat{\omega},t)=\max\limits_{\text{for all } \omega}(H(\omega,t))} \tag{4}$$

with the PIF, temporal variation of dominant nonlinear features of a system, such as a site with liquefaction, can be characterized. Below are two examples.

Figure 1 shows a soil layer configuration and the layout of seismic instruments at Wildlife, California,[15] which was liquefied during the 1987 Superstition Hills earthquake. In the earthquake event, SM2 recorded a ground acceleration time history shown in Fig. 2, while the 5th piezometer, i.e., P5, recorded the excess pore pressure ratio shown in Fig. 3.

According to the recorded pore pressure in Fig. 3, the entire liquefaction process of the liquefiable layer can be divided approximately into three phases: 0–13.5, 13.5–40, and 40–100 s, respectively. The excess pore pressure almost does not generate in the first phase, increases sharply in the second phase, and becomes stable in the last phase. In the second and third phases, a number of time instants appear, marked with numbers in Fig. 3, when the pore pressure drops or dissipates significantly, which may be caused by the instantaneous drainage in the liquefiable layer and the shear dilatancy of the soil medium.

The above liquefaction features can be well related to the temporal variation of the PIF. Figure 4 depicts the PIF time history of the EW-component recording at SM2. It shows that after the onset of liquefaction at 13.5 s, the PIF decreases sharply and subsequently remains at a very low value. Moreover, the local peaks of PIF marked by numbers in Fig. 4 are consistent with the temporal pore-pressure-dissipation at time instants marked in Fig. 3 and the spikes marked in Fig. 2. The above temporal match among the PIF peak, drop of pore pressure and spikes in the acceleration recording is consistent with results obtained by Youd,[16] in which the corresponding time instant is defined as the state shift time of the liquefying layer.

Note that the PIF is also more sensitive to characterizing the liquefaction phenomena in recordings than parameters such as the site average velocity, as validated by comparing Fig. 5 with Figs. 2–4. Figure 5 shows the average shear velocity time history in the top two layers of Fig. 1 estimated on the basis of the acceleration

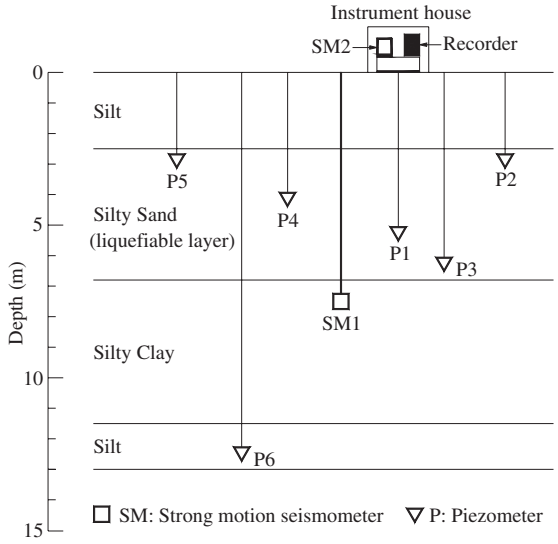

Fig. 1. Wildlife site strata distribution and the layout of seismic instruments at 1987 superstition Hills earthquake.[15]

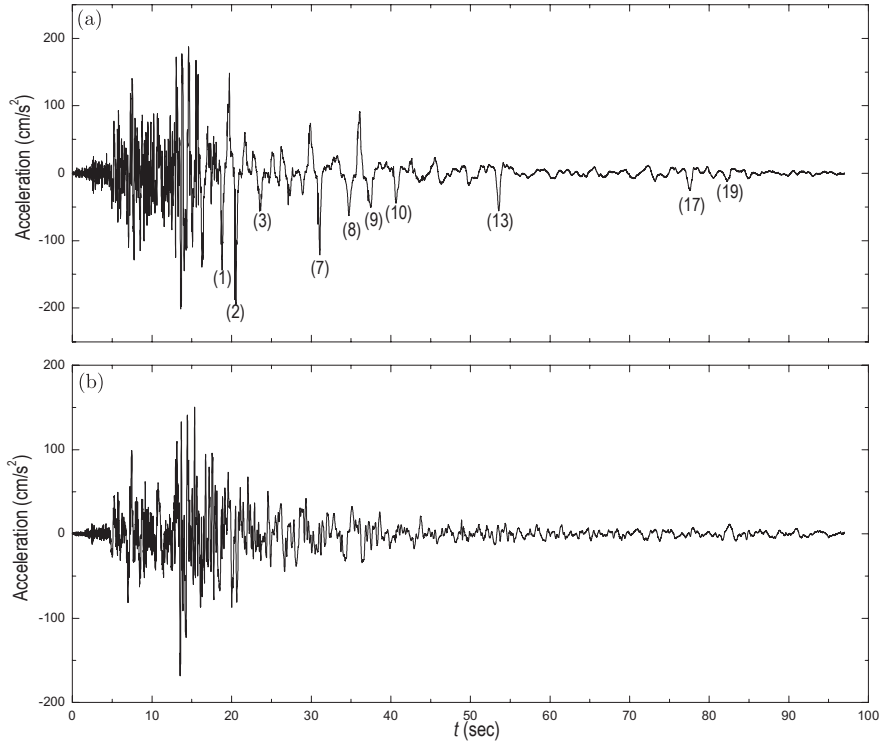

Fig. 2. EW-component acceleration recordings at (a) SM2 and (b) SM1.[16]

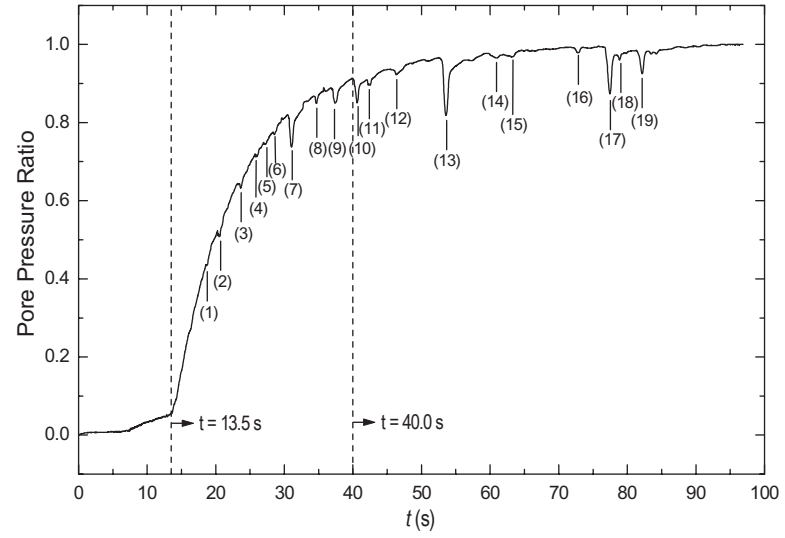

Fig. 3. Excess pore pressure ratio recorded by piezometer P5.[16]

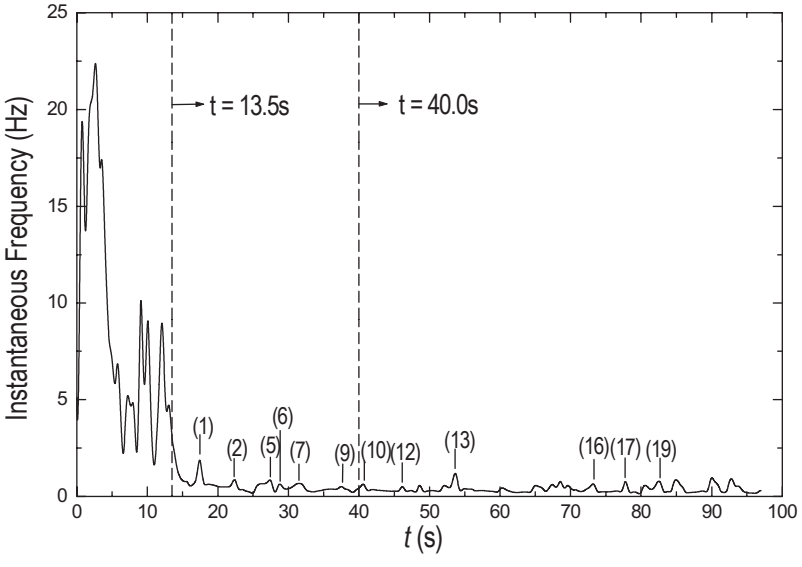

Fig. 4. PIF time history of the EW-component recording at SM2.

recordings at SM1 and SM2 (shown in Fig. 2), with the cross-correlation method proposed by Chang *et al.*[17]

While the above example demonstrates the capability of PIF to depict the liquefaction phenomena in particular and system nonlinear features in general, from

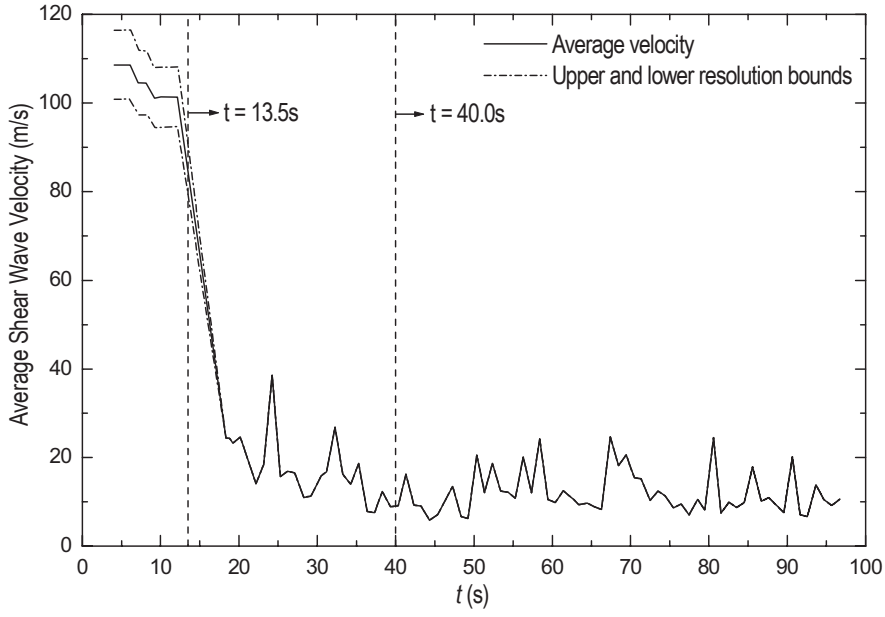

Fig. 5. Average shear velocity time history in layer 1 estimated based on the accelerations recordings at SM1 and SM2 with the cross-correlation method proposed by Chang *et al.*[17]

the acceleration recording at a ground site, the next example shows the distinction between the PIF features of recordings at sites with and without liquefaction.

Figures 6 and 7 show the acceleration recordings at sites with and without liquefaction, respectively. The distinctive motion features in terms of temporal change of the dominant frequency are clearly observed as follows. From the recordings at the liquefaction site plotted in Fig. 6, it shows that the dominant frequencies of the horizontal-component recordings after the onset of liquefaction at around 5–8 s are much lower than those before the liquefaction. The drop of the dominant frequencies in the horizontal-component recordings is much larger than for the vertical component. This liquefaction feature is different from the non-liquefaction site shown in Fig. 7, which illustrates a comparable drop of dominant frequency in both horizontal- and vertical-component recordings.

The above features are well quantified by using the PIF drop and percentage of the PIF level in the entire time period of the strong motion, depicted in Figs. 8 and 9, respectively. In particular, Fig. 8 shows that the PIF drop after the liquefaction in the horizontal-component recordings is much larger than the vertical component. The percentage of the time duration with PIF below 1.0 Hz over the entire time period of the strong motion in the horizontal-component recordings is also much larger than the vertical component, which is an alternative measure of liquefaction features in recordings. In contrast, Fig. 9 shows that the percentage of time duration for PIF below 1.0 Hz with non-liquefied soil is consistent with

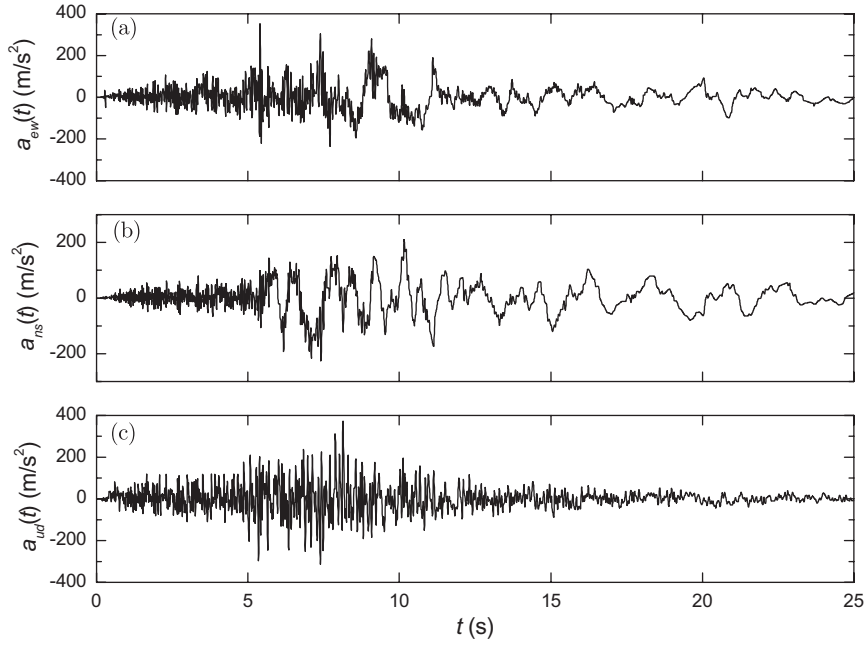

Fig. 6. (a) EW- (b) NS- and (c) UD-component acceleration recordings of the 1995 Kobe earthquake at Amagasaki PPKE3 (liquefied site) in Japan.

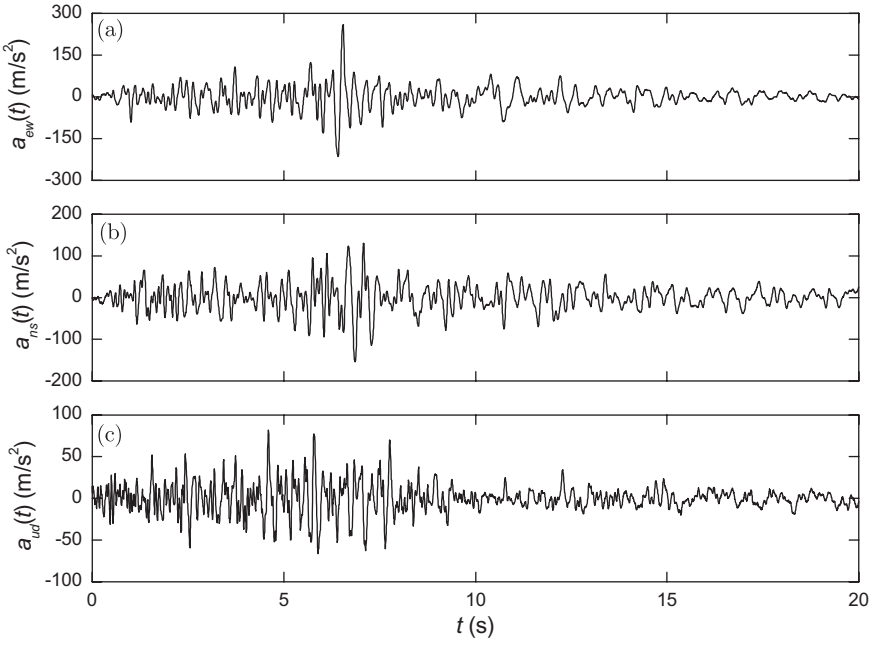

Fig. 7. (a) EW- (b) NS- and (c) UD-component acceleration recordings of the 1994 Northridge earthquake at LA Bell Postal Facility (stiff soil site) in USA.

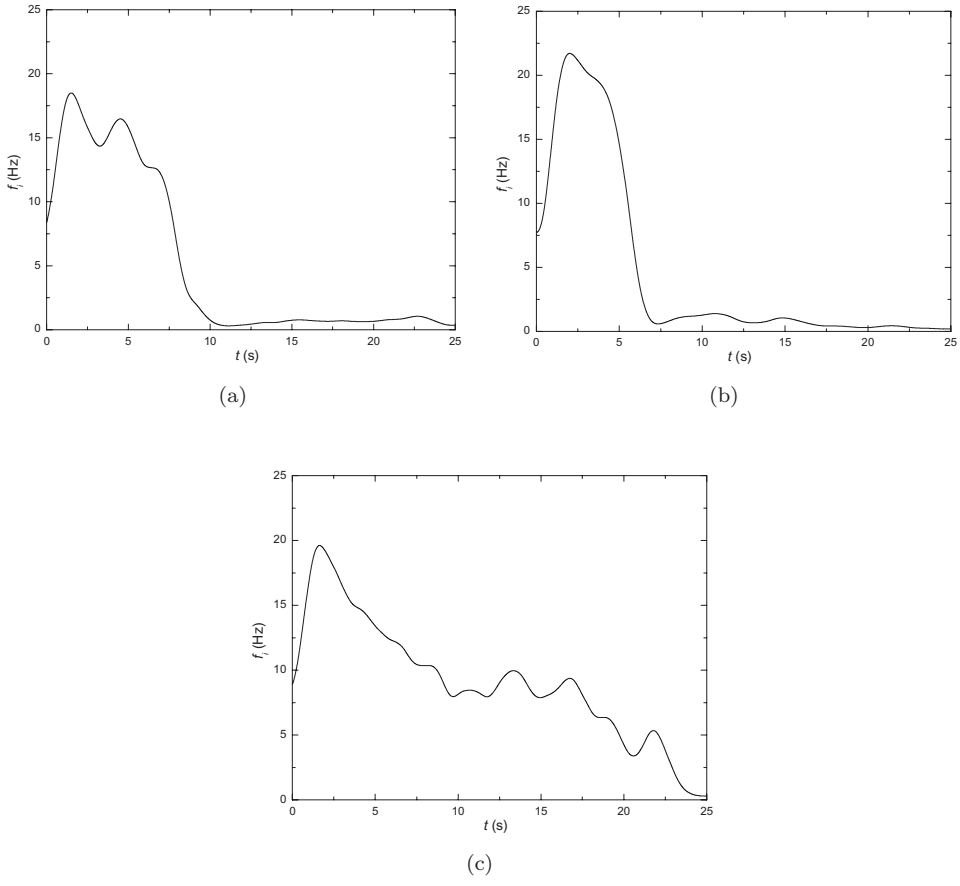

Fig. 8. Time histories of predominant instantaneous frequency (PIF) of acceleration recordings at liquefied site in Fig. 9 in (a) EW component, (b) NS component, and (c) UD component.

each other in both horizontal- and vertical-component recordings, different from the features in the liquefaction site.

The above analysis suggests that the percentage of the time duration of the PIF level in the entire time history can be used as an index to diagnose site conditions with or without liquefaction. Note that the percentage of the time duration of the PIF used in the above example, instead of the time duration of PIF, eliminates the influences of source, since different sources will have different total and sub durations. To this end, two PIF-related ratios are introduced below:

$$R_{h,f} = \frac{1}{2}\left[\frac{T_{h1,f}}{T_d} + \frac{T_{h2,f}}{T_d}\right], \tag{5}$$

$$R_{v,f} = \frac{T_{v,f}}{T_d}, \tag{6}$$

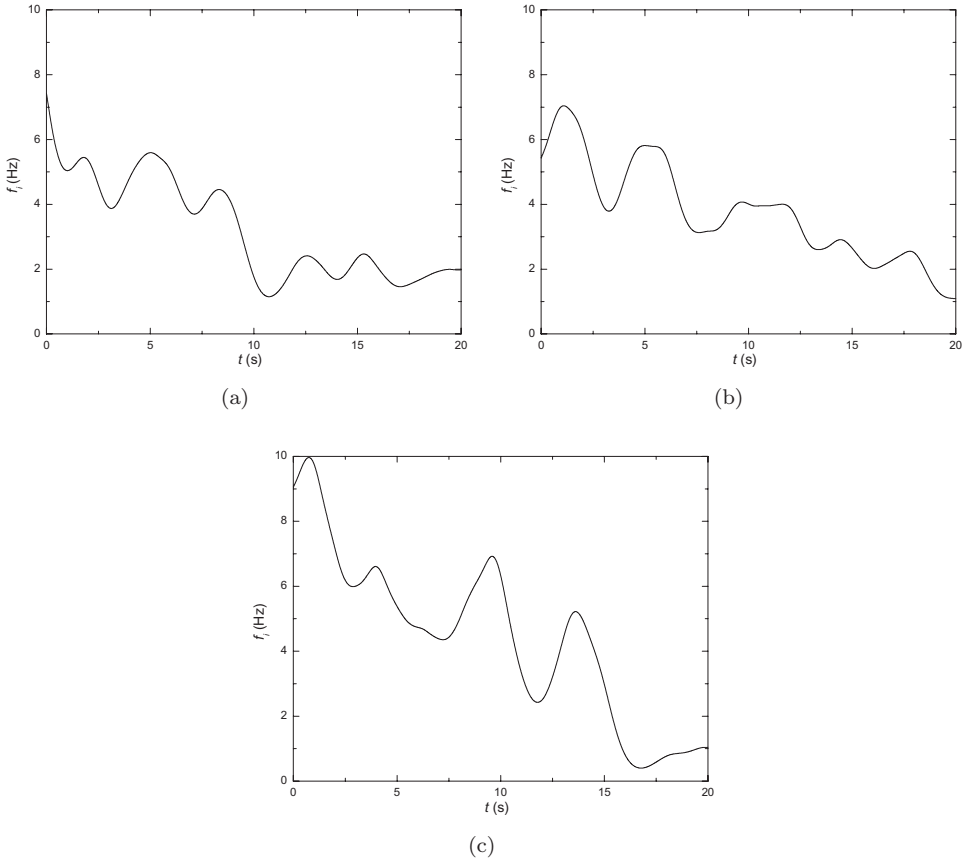

Fig. 9. Time histories of predominant instantaneous frequency (PIF) of acceleration recordings at stiff soil site in Fig. 10 in (a) EW component, (b) NS component, and (c) UD component.

where $T_{hi,f}$ ($T_{v,f}$) is the time duration with the PIF of ith horizontal (vertical) recording below a threshold value f, and T_d is the time duration of the strong motion (e.g., Hu *et al.*[18]).

With the PIF-related ratios, a recording-based liquefaction-detection approach is proposed as follows:

1. If $R_{h,0.6} > 0.4$ and $R_{v,1.0} > 0.4$, the site is identified as liquefaction, denoted with number 1;
2. If the above condition is not satisfied but $R_{h,1.0} > 0.4$ and $R_{v,1.0} > 0.4$, the site is identified as liquefaction-suspicious, denoted with number 0.5;
3. Otherwise, the site is not liquefied with number 0.

Note the parameters used in the above, such as the threshold value of frequency of 0.6, are selected on the basis of this and other pertinent studies (e.g., Refs. 13 and 14).

3.3. *Numerical analysis and comparison*

To validate the effectiveness of the proposed detection approach, 29 seismic recordings selected from well-examined common data sets were analyzed. The results were compared with those from post-event damage investigations and from the liquefaction detection methods of Kostadinov and Yamazaki[14] and Suzuki *et al.*[13]

Tables 1 and 2 list the information about recording site, earthquake event, damage investigation results, and results obtained from Suzuki's, Kostadinov's, and proposed methods. It shows that the proposed method is more effective in detecting the liquefaction sites than the others methods.

Since Suzuki's method is applied to the horizontal-component recordings only, lack of the vertical-component recording information leads to the misdetection of some non-liquefied soil sites as liquefied ones, as exemplified by sites 3, 4, and 6. Moreover, Suzuki's method cannot differentiate between the liquefied and the

Table 1. Results of liquefaction detection with different approaches, in which 1 denotes detection result of liquefaction (LIQ), 0 is detection result of non-liquefaction (NON), 0.5 represents the detection result of liquefaction-suspicion (SUS), as well as their comparison with the results of site liquefaction condition obtained with *in-situ*, post-earthquake site investigation.

No.	Site	Damage investigation	Suzuki method	Kostadinov method	Proposed method
1	Kawagishi-Cho	LIQ	0	0	1
2	Aomori Harbor	LIQ	1	1	1
3	C. de Abastos Frigorifico	NON	1	0	0
4	Secretaria Communication & Tran.	NON	1	0	0
5	Tacubaya, D. F.	NON	0	0	0
6	Tlahuac Bombas	NON	1	0	0
7	Wildlife GL	LIQ	1	1	1
8	LA, Bell Postal Facility, Ground	NON	0	0	0
9	LA, Griffith Observatory	NON	0	0	0
10	LA, Sepulveda Canyon, Ground	NON	0	0	0
11	LA, Wadsworth VA Hosp., South Site	NON	0	0	0
12	Pasadena, 535 South Wilson Ave.	NON	0	0	0
13	Topanga, Fire Station, Ground	NON	0	0	0
14	Amagasaki, Bridge GR-2	SUS	1	1	0.5
15	Amagasaki-G	LIQ	1	1	1
16	Amagasaki No. 3 P. P., KE	LIQ	1	1	1
17	Higashi-Kobe Bridge	LIQ	1	1	1
18	Kobe, JMA	NON	0	0	0
19	Kobe-Dai8-G	LIQ	1	0.5	1
20	Kobe-JI-S	LIQ	1	1	1
21	Kobe University, CEORKA	NON	0	0	0
22	Port Island GL	LIQ	1	1	1
23	Port Island GL-16	LIQ	0	0.5	0.5
24	Port Island GL-32	SUS	0	0.5	0.5
25	Port Island GL-83	NON	0	0	0
26	Rokko Island City, B3, BIF	LIQ	1	1	1
27	Shin Kobe S. S., KE	NON	0	0	0
28	JR Takarazuka Station	NON	0	0	0
29	JR Takatori Staion	SUS	1	0.5	0.5

Table 2. Earthquake events with different sites.

Site no.	Event	Date
1	Japanese Niigata earthquake	16 June 1964
2	Japanese Honshu earthquake	16 May 1968
3∼6	Mexican Michoacan earthquake	19 September 1985
7	American Superstition Hills earthquake	24 November 1987
8∼13	American Northridge earthquake	17 January 1994
14∼29	Japanese Kobe earthquake	17 January 1995

liquefaction-suspicious sites, as shown in sites 14, 24, and 29. While Kostadinov's method improves the effectiveness, exemplified by detecting the liquefaction condition of sites 3, 4, 6, 24, and 29, it still makes wrong detection, notably at site 1 which is a well-known liquefaction site. In contrast, the proposed method more accurately detects the liquefaction site condition than the other two methods, as exemplified by sites 1, 14, and 19. In addition, results obtained with the proposed method are consistent with the damage investigation results, except at site 23, where both proposed and Kostadinov's methods show the same result, but are still better than Suzuki's method.

In addition to effectively detecting liquefaction, the proposed method differentiates site conditions with non-liquefaction soft soils from those with stiff soil. Figure 10 shows a plot of $R_{h,1.0}$ and $R_{v,1.0}$ for the 29 data sets. It shows that

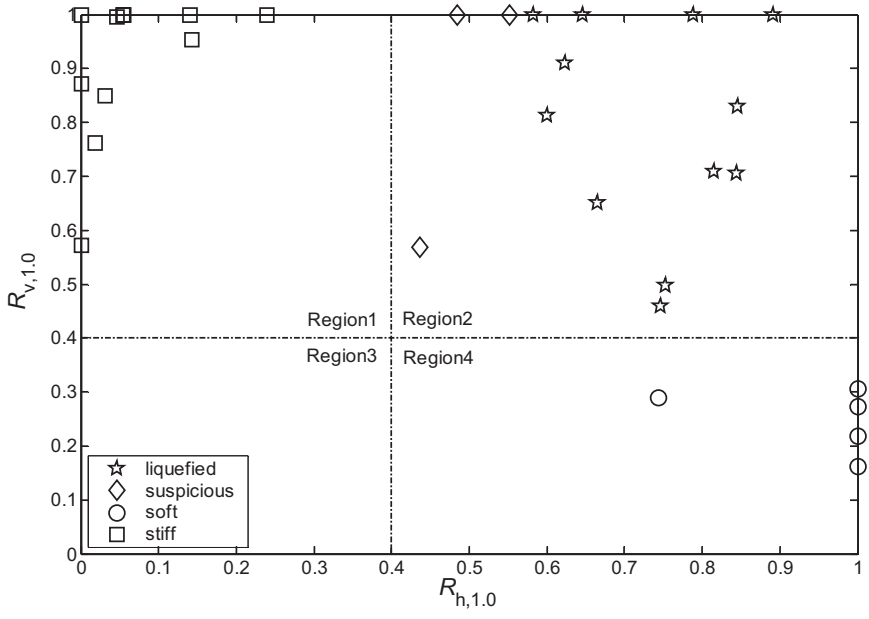

Fig. 10. Plot of $R_{h,1.0}$ and $R_{v,1.0}$ for the 29 data sets, aid in differentiating liquefaction and liquefaction-suspicious sites from non-liquefaction sites with stiff and soft soil.

the data sets that fall in Region 1 of $R_{h,1.0} < 0.4$ and $R_{v,1.0} > 0.4$ correspond to non-liquefaction stiff-soil sites, those in Region 2 of $R_{h,1.0} > 0.4$ and $R_{v,1.0} > 0.4$ represent the liquefied or liquefaction-suspicious sites, and those in Region 4 of $R_{h,1.0} > 0.4$ and $R_{v,1.0} < 0.4$ are associated with the non-liquefaction soft-soil sites.

4. Soil Nonlinearity and Influences in Site Amplification

4.1. *Background*

The influences of soil nonlinearity in ground motion response are typically discerned and analyzed with the aid of FSA of the recordings. In particular, two sets of recordings for mainshock and aftershock are needed, i.e., one at a soil site and the other at a referenced site such as bedrock or outcrop. The Fourier spectral ratio for an earthquake event, termed as Fourier-based site-amplification factor, is then defined as the ratio of Fourier amplitude spectra of the recordings at the two sites. Since the wave paths and earth structures excluding the soil layer(s) near the surface are almost the same for the soil and referenced sites, the Fourier-based, site-amplification factor eliminates approximately the influences of source from the earthquake event and thus provides essentially the dynamic characteristics of the site. In addition, the recordings at the referenced site are generally believed as the results of linear wave responses and the recordings at the soil site subjected to the large-amplitude mainshock, but not to the small-amplitude aftershock, are the results of nonlinear wave responses. Accordingly, comparing the site-amplification factors from the mainshock and the aftershock could help explore and quantify the site nonlinearity.

Consensus has been building that the site-amplification factors in the current codes overemphasize the extent of soil nonlinearity, and thus potentially underestimate the level of site amplification. This aspect is demonstrated in Borcherdt[19] that the recording-based site amplification factors are larger than those in codes for a certain range of base acceleration intensity. In addition, some features of site-amplification factors used in codes and guidance for structural design contradict findings from the 1994 Northridge ground motion data sets.[20] Since seismic ground motion recordings with liquefaction in the soil layers near the surface typically show similar, but strong nonlinear features of those with soil nonlinearity, the aforementioned consensus and findings will also be applicable to the FSA-based characterization of liquefaction.

The aforementioned problem might be partly because seismologists and engineers lack sufficient understanding of the underlying causes in nonlinearity. For example, the influence of soil heterogeneity does not scale linearly even when the soil is perfectly linear.[21] In other words, a linear elastic medium with random heterogeneity can change ground motion in a way similar to that caused by medium nonlinearity. Consequently, it is possible for one to interpret the motion influenced by random heterogeneous media as soil nonlinearity (e.g., Yoshida and Iai[22]), which can distort the quantification of site amplification. The problem may also partly

because there is lack of an effective approach to properly characterize nonlinear features of ground motion in recordings and then to quantify them.

4.2. *HHT-based site amplification and damping*

Alternative to Fourier-based approach, an HHT-based approach for characterizing nonlinear site amplification is proposed that is similar to Fourier-based approach. The HHT-based site-amplification factor (FH) is defined

$$FH_s(\omega) = \frac{\sqrt{h_{s,h1}^2 + h_{s,h2}^2}}{\sqrt{h_{r,h1}^2 + h_{r,h2}^2}}, \tag{7}$$

where $h(\omega)$ is marginal Hilbert amplitude spectrum of the data, subscripts s and r denote, respectively the soil and reference sites, and subscripts $h1$ and $h2$ denote the two horizontal components. While the above HHT-based site amplification can provide an alternative insight in characterizing and quantifying the site nonlinearity, the role of damping in nonlinear site responses is not discerned from the general features of site nonlinearity, which should be implicitly involved in the factor.

To single out the influences of site damping from the HHT-based site amplification in Eq. (7) that is associated with amplitude $a_j(t)$ in Eq. (1), the physical meanings of the jth IMF component that forms the amplitude $a_j(t)$ is first examined below. Since all the IMF components are extracted from acceleration records that are the result of seismic waves generated by a seismic source and propagating in the earth, they should reflect the wave characteristics inherent to the rupture process and the earth medium properties.

Indeed, with the aid of a finite-fault inversion method, signature of the seismic source of the 1994 Northridge earthquake is examined in the large-amplitude IMF components of the ground acceleration recordings.[23] That study only looks over the second to fifth IMF components because they are much larger in amplitude than the remaining higher-order, low-frequency IMF components. The first IMF component was not investigated in the above study because it contains information that is not simply or easily related to the seismic source (e.g., wave scattering in the heterogeneous media). That study shows that the second IMF component is predominantly wave motion generated near the hypocenter, with high-frequency content that might be related to a large stress drop associated with the initiation of the earthquake. As one progresses from the second to the fifth IMF component, there is a general migration of the source region away from the hypocenter with associated longer-period signals as the rupture propagates. In addition, that study shows that some IMF components (e.g., the fifth IMF) can exhibit motion features reflecting the influences of nonlinear site condition.

Because of the relationship of IMF components to the source, Eq. (1) is re-written as

$$X(t) = \Re \sum_{j=1}^{n} a_j(t) e^{i\theta_j(t)} = \Re \sum_{j=1}^{n} \Lambda_j(t) e^{-\varphi_j(t) + i\theta_j(t)}, \tag{8}$$

where time-dependent amplitudes $\Lambda_j(t)$ can be interpreted as the source-related intensity, $\varphi_j(t)$ are the exponential factors characterizing the time-dependent decay of the waves in the jth IMF component due to damping, and

$$a_j(t) = \Lambda_j(t) e^{-\varphi_j(t)}. \tag{9}$$

Similar to instantaneous frequency, Hilbert and marginal Hilbert spectra in Huang *et al.* (1998), the instantaneous damping factor, Hilbert and marginal Hilbert damping spectra can be defined, respectively as (see Ref. 6)

$$\eta_j(t) = \frac{d\varphi_j(t)}{dt}, \tag{10}$$

$$D(\omega, t) = \sum_{j=1}^{n} \eta_j(t) = \sum_{j-1}^{n} \left[-\frac{\dot{a}_j(t)}{a_j(t)} + \frac{\dot{\Lambda}_j(t)}{\Lambda_j(t)} \right], \tag{11}$$

$$d(\omega) = \int_0^T D(\omega, t) dt = \sum_{j=1}^{n} \int_0^T \left[-\frac{\dot{a}_j(t)}{a_j(t)} + \frac{\dot{\Lambda}_j(t)}{\Lambda_j(t)} \right] dt = d^a(\omega) + d^\Lambda(\omega). \tag{12}$$

Equation (12) indicates that the marginal Hilbert damping spectrum consists of two terms: one is from the time-dependent amplitudes $a_j(t)$ that are related to marginal and Hilbert amplitude spectra, and the other from source-related intensity, i.e., time-dependent amplitudes $\Lambda_j(t)$.

For recordings to an earthquake, Λ_j is unknown, dependent upon source and time. The influences of Λ_j in the site damping, however, can be removed if two sets of recordings at soil and referenced sites are used. Similar to the HHT-based site amplification, the difference of marginal Hilbert damping spectra at soil and referenced sites, or named similarly as HHT-based site damping, can approximately eliminate the influences of source that is associated with Λ_j and thus provide essentially the characterization of the site damping. The HHT-based site damping can be found as

$$\begin{aligned} d_\Delta(\omega) &= \sqrt{[d_{s,h1}(\omega) - d_{r,h1}(\omega)]^2 + [d_{s,h2}(\omega) - d_{r,h2}(\omega)]^2} \\ &\approx \sqrt{[d^a_{s,h1}(\omega) - d^a_{r,h1}(\omega)]^2 + [d^a_{s,h2}(\omega) - d^a_{r,h2}(\omega)]^2}, \end{aligned} \tag{13}$$

where use has been made in the last approximation that the source-related damping terms at the soil and referenced sites are approximately equal, i.e., $d^\Lambda_s(\omega) \approx d^\Lambda_r(\omega)$.

Finally, comparing the HHT-based site amplification and damping from the mainshock and the aftershock can help quantify the site nonlinearity.

4.3. *Numerical example*

Shown in the section, the proposed approach is used to analyze the recordings of the M6.8 mainshock and the M_L3.4 aftershock of the 2001 Nisqually earthquake at four soft and four stiff soil sites.

This study first examines the site nonlinearity at SDS, a soft soil site on artificial fill with nearby liquefaction and the average shear-wave velocity in the top 30 m is Vs30 = 148 m/s, and the stiff soil site LAP, which is over a stiff soil with Vs30 = 367 m/s. Recordings at SEW are used as referenced-site ones, because SEW has Vs30 = 433 m/s that is within the range of Vs30 values for typical rock sites in the western US, which is also used so in Fourier-based studies (e.g., Frankel *et al.*[24]).

Figures 11 and 12 show, respectively two horizontal acceleration recordings of the aftershock and mainshock at site SEW, while Figs. 13 and 14 depict the corresponding recordings at SDS. Comparing these figures indicates that the aftershock contains motion with smaller amplitude and richer high frequency than the mainshock. This is primarily due to the influences of source, for the wave

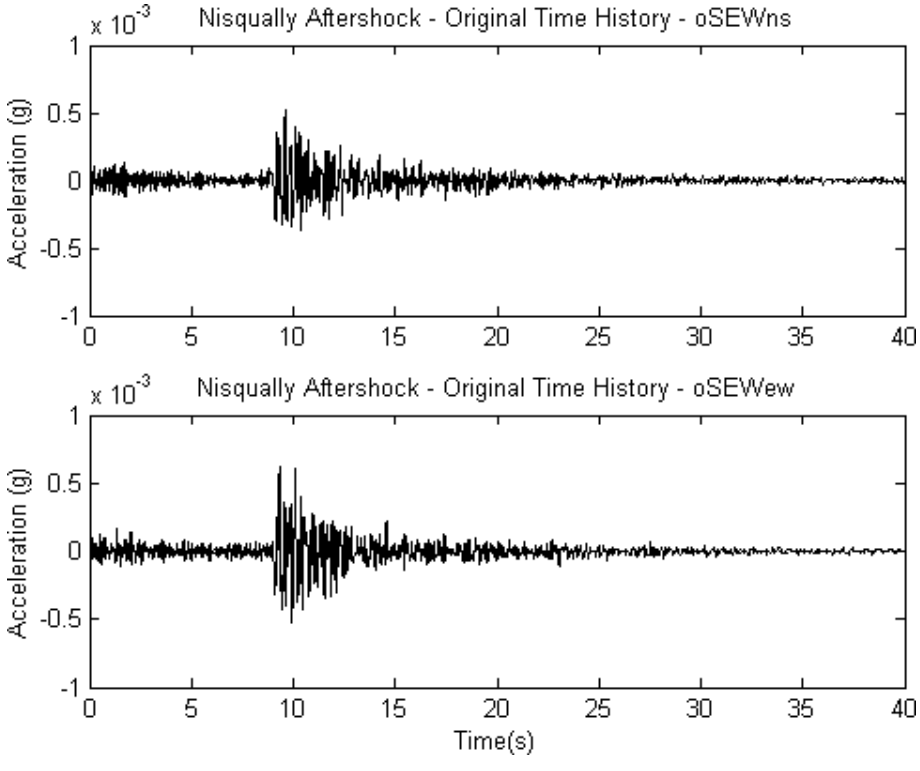

Fig. 11. Time histories of two horizontal acceleration components for aftershock of the 2001 Nisqually earthquake at SEW.

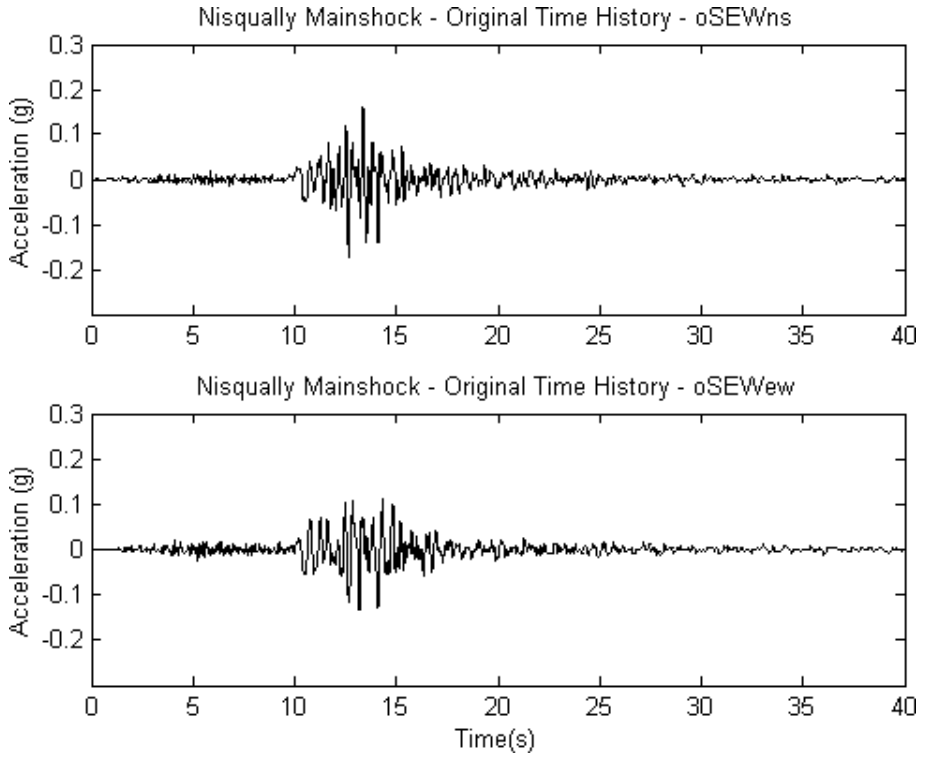

Fig. 12. Time histories of two horizontal acceleration components for mainshock of the 2001 Nisqually earthquake at SEW.

paths are almost the same at the given sites. The aftershock is typically generated over a ruptured fault much smaller than the mainshock, consequently yielding the smaller-amplitude, higher-frequency aftershock motion than the mainshock motion. Contrasting Figs. 12 and 14 also illustrates much lower-frequency, larger-amplitude mainshock motion after the S-wave arrival at about 10 s at SDS than at SEW. This is caused not only by the site difference of soft soil versus rock, but also by the difference of strong site nonlinearity versus site linearity. The indication of site nonlinearity in recordings at SDS can be further confirmed with the existence of abnormal, large-amplitude, high-frequency spikes in 20–25 s in the mainshock at SDS in Fig. 14. The above abnormal spikes and waveform have been concluded[24] as symptomatic of nonlinear response at the soft soil site.

Figure 15(a) shows the HHT-based site-amplification factors of the mainshock and aftershock at SDS. In calculating the factors (and subsequent HHT-based site amplification and damping), the correction for $1/R$ geometrical spreading in the recordings at SDS and SEW is not carried out since the hypocentral distances for the sites under investigation are similar. In addition, the marginal amplitude

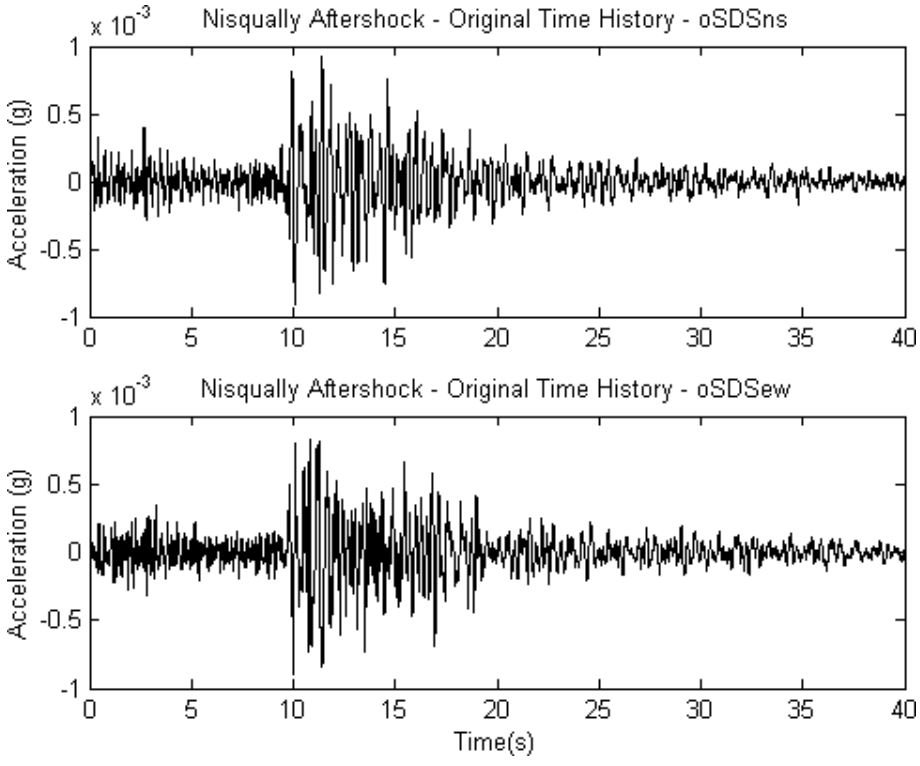

Fig. 13. Time histories of two horizontal acceleration components for aftershock of the 2001 Nisqually earthquake at SDS.

spectra are not smoothed in the calculation, for the non-smoothed spectra more clearly show the characteristics of the HHT-based approach. Examining Fig. 15(a) shows the following:

1. The profile of the HHT-based factor in the frequency band up to 2.5 Hz (referred to as low-frequency range) is generally downshifted in frequency from the aftershock to the mainshock. For example, the profile of the aftershock in 1–2 Hz is downshifted to that of the mainshock with an average shift of approximately 0.36 Hz (see Fig. 15(c)).
2. The profile of the HHT-based factor in the frequency band 2.5–7 Hz (intermediate-frequency range) is generally reduced in amplitude from the aftershock to the mainshock. For example, the profile of the aftershock in 3–4 Hz with an averaged-amplitude for the factor 7.26 is downshifted to 3.00 for the mainshock, yielding the amplitude-reduction factor of $0.41 = 3.00/7.26$ (see Fig. 15(c)).
3. There is no evidence to support a difference in the factor starting at 7–10 Hz (high-frequency range) between the mainshock and aftershock.

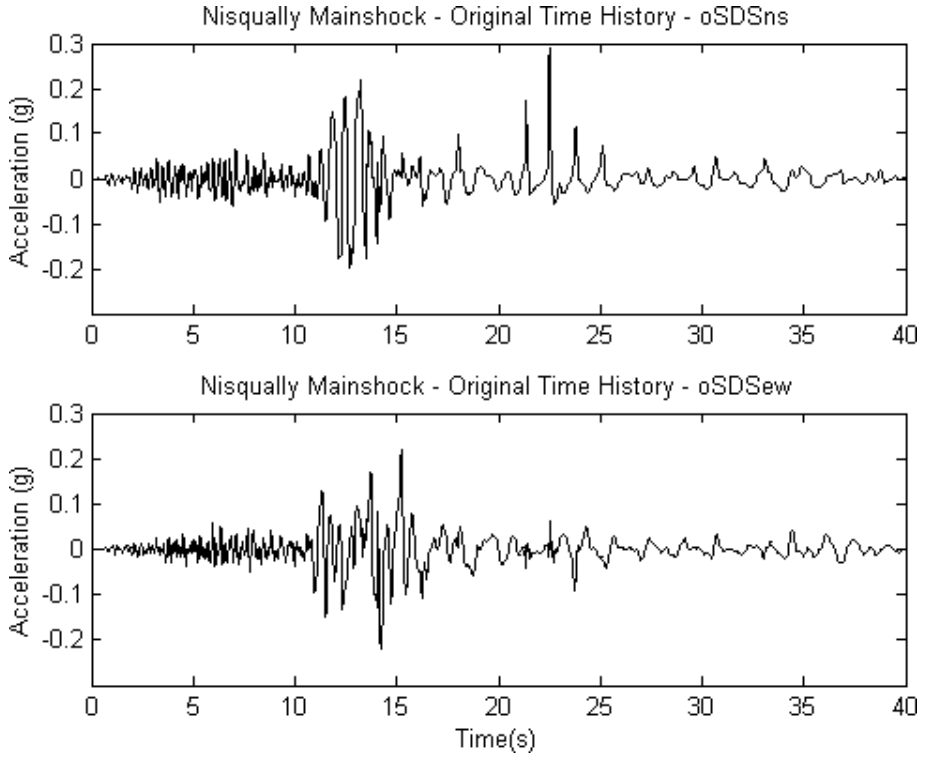

Fig. 14. Time histories of two horizontal acceleration components for mainshock of the 2001 Nisqually earthquake at SDS.

In contrast, the HHT-based factors of the mainshock and aftershock at stiff soil site LAP are shown in Fig. 16(a), which demonstrates the following.

1. In the low-frequency range (below 2.5 Hz), Fig. 16(a) shows a downshift profile in both frequency and amplitude from the aftershock to mainshock that is similar to Fig. 15(a) in the low-to-intermediate frequency range, but Fig. 8(a) shows a smaller frequency downshift (e.g., 0.16 Hz in 1–2 Hz) than the latter (0.36 Hz in 1–2 Hz) in the same frequency band.
2. In the intermediate-to-high frequency range, there is almost no difference in the two factors between the mainshock and the aftershock.

With the frequency downshift and amplitude-reduction factor as the measure for the degree of site nonlinearity, comparison of the HHT-based factors at SDS and LAP suggests that SDS has strong site nonlinearity during the mainshock, and LAP has weak site nonlinearity. Site LAP can also be regarded as having almost no site nonlinearity under the mainshock if the aforementioned small downshift in both frequency and amplitude in the low-frequency range is the result of variation of data collection and sampling.

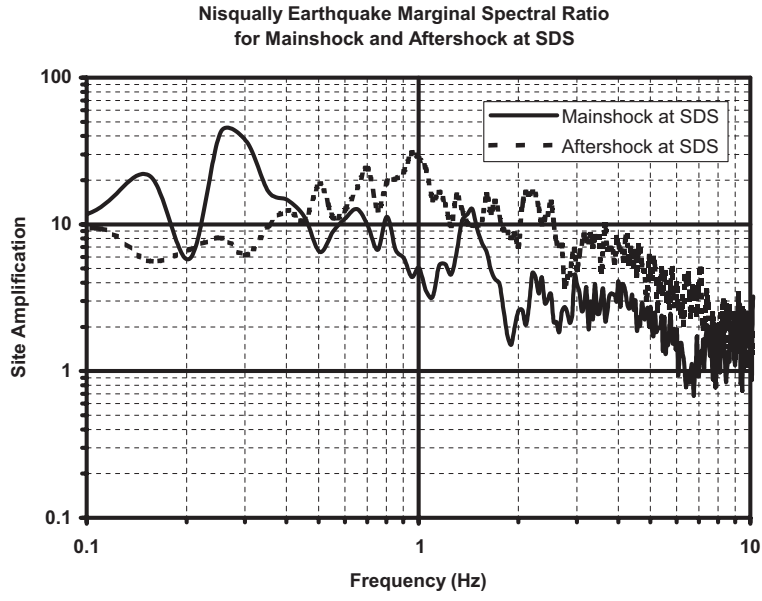

(a)

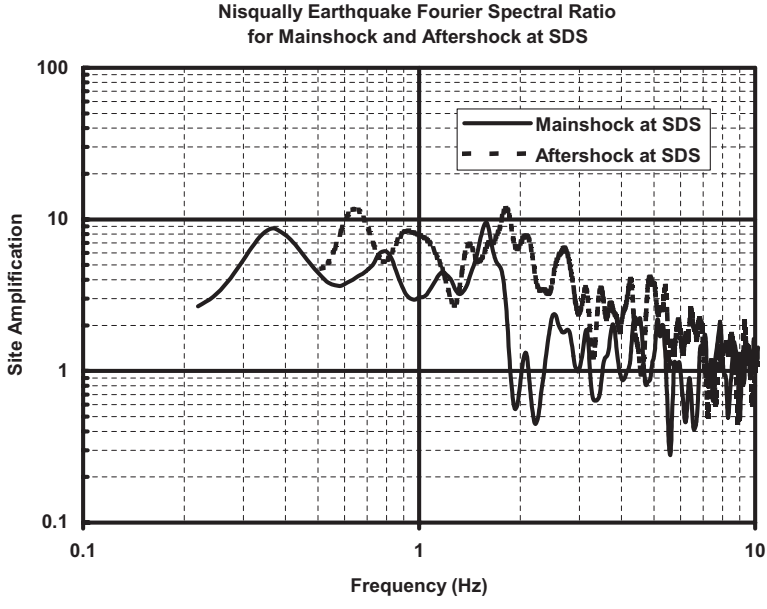

(b)

Fig. 15. (a) HHT-based site amplification at soft soil site SDS for mainshock and aftershock of the 2001 Nisqually earthquake. (b) Fourier-based site amplification at soft soil site SDS for mainshock and aftershock of the 2001 Nisqually earthquake. (c) Illustrated measurement for averaged frequency downshift in the 1–2 Hz band and averaged amplitude reduction in the 3–4 Hz band from the HHT-based site amplification in (a).

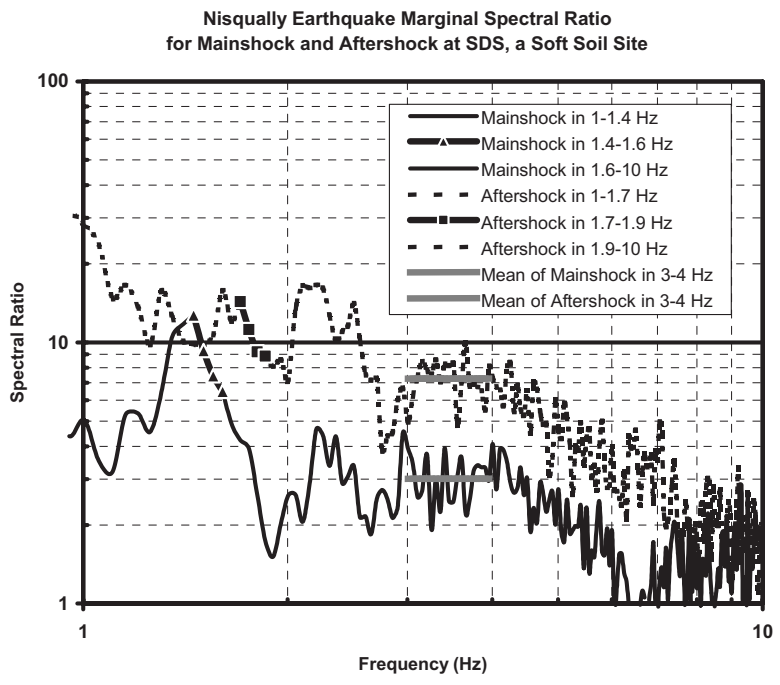

(c)

Fig. 15. (*Continued*)

To illustrate the characteristics of the HHT-based approach, this study compares the HHT-based site-amplification factors in Figs. 15(a) and 16(a) with Fourier-based ones in Fig. 15(b) and 16(b) (i.e., Fig. 7 in Ref. 24), revealing the following.

1. In the low-frequency range, Fig. 15(b) shows a frequency-downshift profile from the aftershock to mainshock that is similar to Fig. 15(a), but the former shows a smaller shift (about 0.21 Hz) than the latter (about 0.36 Hz) in frequency range 1–2 Hz. Because of the distortion characteristic in Fourier spectral analysis for nonlinearity-related nonstationary data as indicated in Sec. 3, the frequency downshift measured from the HHT-based factors in Fig. 15(a) may give a more truthful indication of the site nonlinearity than that from the Fourier-based factors in Fig. 15(b). In addition, the factors in the low-frequency range in Fig. 15(a) are generally somewhat larger than those in Fig. 15(b).
2. In the intermediate-frequency range, Fig. 15(b) shows an amplitude-reduction profile from the aftershock to mainshock that is similar to Fig. 15(a), but Fig. 15(b) shows a relatively smaller reduction with more oscillation than Fig. 15(a) (e.g., an averaged amplitude-reduction factor of $0.49 = 1.22/2.48$ in 3–4 Hz for Fig. 15(b) and $0.41 = 3.00/7.26$ for Fig. 15(a)).

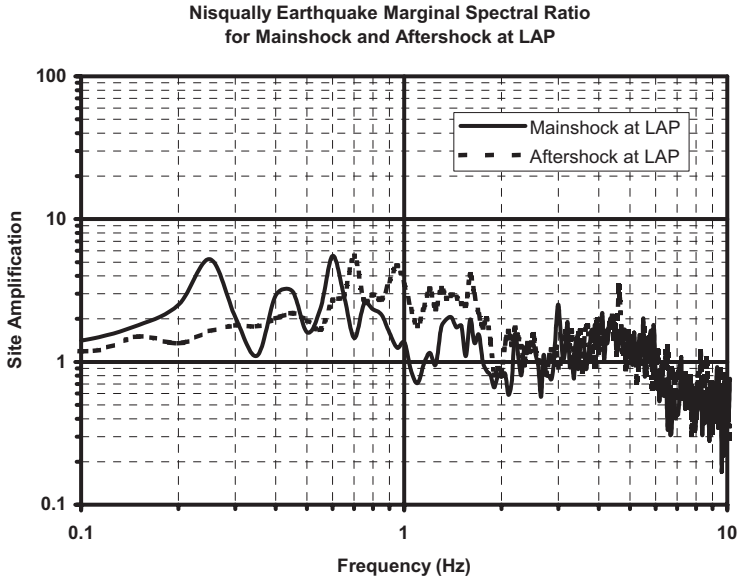

(a)

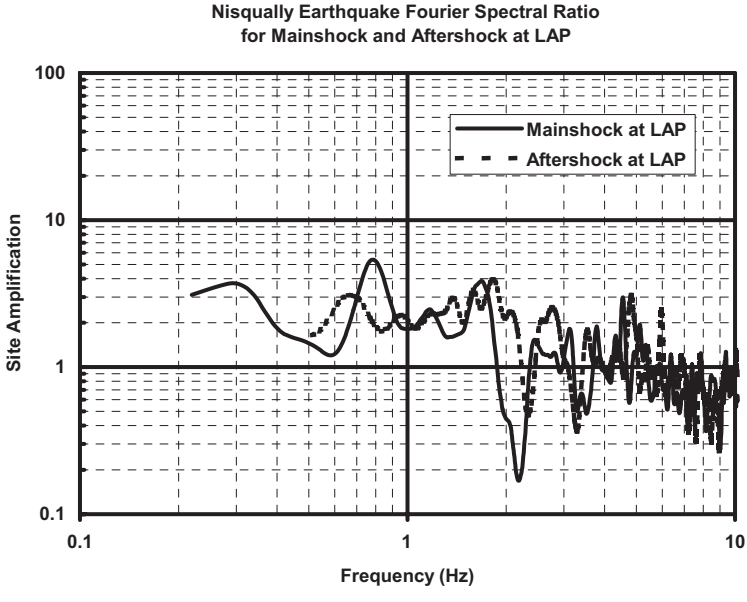

(b)

Fig. 16. (a) HHT-based site amplification at stiff soil site LAP for mainshock and aftershock of the 2001 Nisqually earthquake. (b) Fourier-based site amplification at stiff soil site LAP for mainshock and aftershock of the 2001 Nisqually earthquake.

3. Almost no essential difference is observed from Figs. 16(a) and 16(b) in terms of overall profile, amplitude of site-amplification factor, and frequency downshifts between the mainshock and aftershock, except the amplitude change in 1–2 Hz, implying that the two approaches are almost consistent with each other in characterizing linear phenomena and estimating weakly-nonlinear site amplification.

To support the above observations, the site amplifications at three other soft soil sites (i.e., HAR, BOE, and KDK) and three other stiff soil sites (i.e., BHD, THO, and SEU) of the Nisqually earthquake are calculated. Note that all the Fourier spectral ratios are taken from Frankel *et al.*[24] The results at each and every site are similar to the above.

Figures 17 and 18 show, respectively, the HHT-based and Fourier-based site amplifications for mainshock and aftershock averaged over four soft and four stiff soil sites. Table 3 summarizes peak ground acceleration, frequency downshift in 1–2 Hz, and amplitude-reduction factor in 3–4 Hz at each site, as well as the averaged value over four soft and four stiff soil sites. The statistical results for site amplification and nonlinearity characterization in Figs. 17 and 18 and Table 3 are essentially consistent to those at each individual site, suggesting that HHT-based approach is equivalent to Fourier-based one in quantifying weakly nonlinear or linear site amplification, but more effective in quantifying strong site nonlinearity in terms of frequency downshift and amplitude-reduction factor than Fourier-based one.

As an alternative, complementary characterization of site nonlinearity, Figs. 19 and 20 show, respectively, the HHT-based site damping at soft soil site SDS and stiff soil site LAP.

Figure 19 reveals that the site damping at SDS in the mainshock is much larger than that in the aftershock at frequency up to about 5 Hz, suggesting that strong site nonlinearity occurred during the mainshock in the frequency band. The increased damping will reduce the amplified seismic wave responses through the nonlinear soil and thus reduce the site-amplification factor, with the quantities at the linear soil used as a reference. This can be confirmed from Fig. 7(a), which shows that the HHT-based factor for site amplification is observably reduced for the mainshock from the aftershock in the similar frequency band of 0.4–7 Hz.

In comparison, Fig. 20 shows that the site damping at LAP is essentially the same between mainshock and aftershock events, suggesting that site LAP is linear or weakly nonlinear for both events. This is consistent with the observations from the site-amplification factors in Figs. 20(a) and 20(b).

Figures 21 and 22 show the HHT-based site damping averaged over four soft and four stiff soil sites. It can be seen that the site damping at soft soil site in the mainshock is larger than that in the aftershock in frequency around 0.8–3 Hz, and the site damping at stiff soil site in the mainshock is larger than that in the aftershock in frequency around 1 Hz. The site damping in the rest frequency range except very low frequency remains almost the same. This suggests in general that

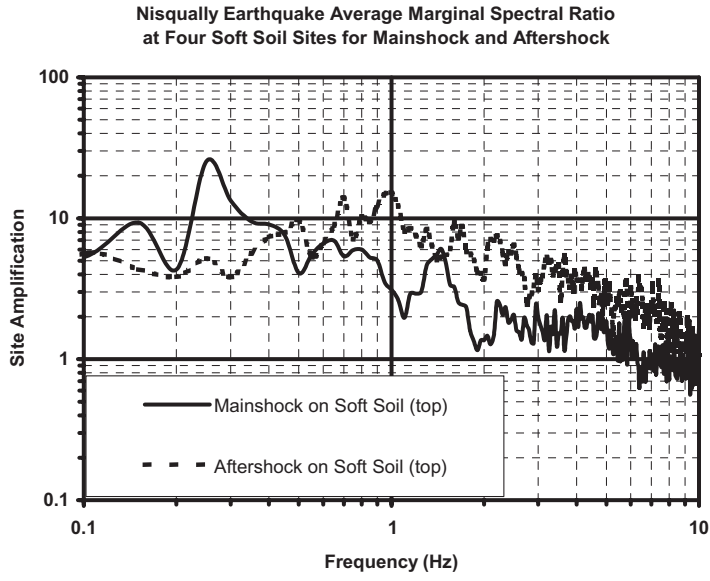

(a)

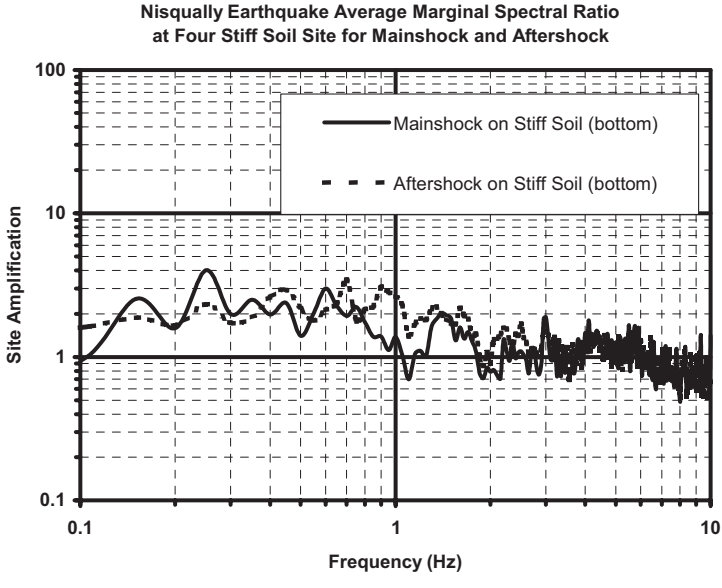

(b)

Fig. 17. (a) Averaged HHT-based site amplification over four soft soil sites for mainshock and aftershock of the 2001 Nisqually earthquake. (b) Averaged HHT-based site amplification over four stiff soil sites for mainshock and aftershock of the 2001 Nisqually earthquake.

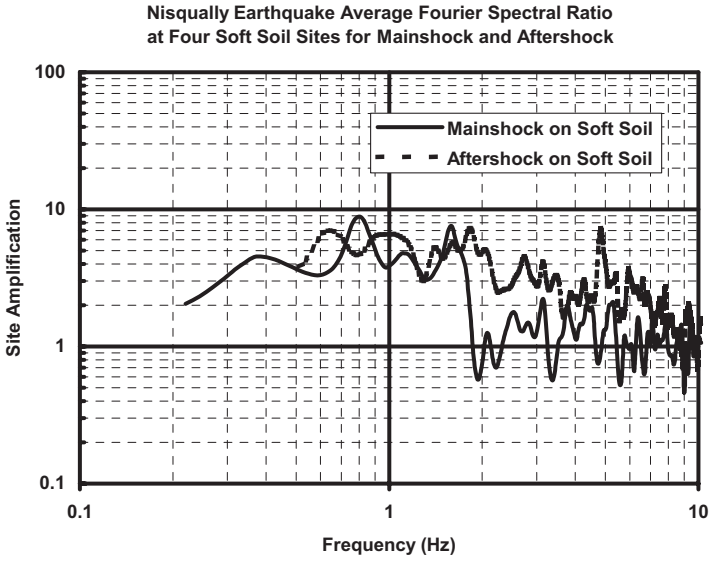

(a)

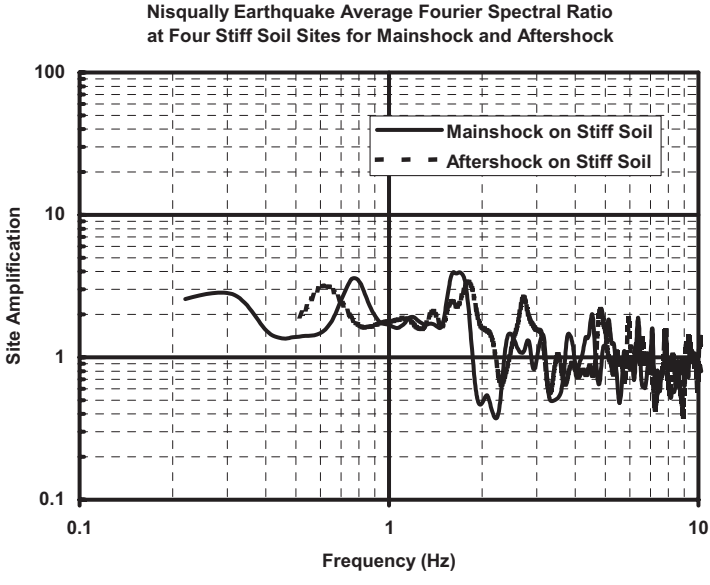

(b)

Fig. 18. (a) Averaged Fourier-based site amplification over four soft soil sites for mainshock and aftershock of the 2001 Nisqually earthquake. (b) Averaged Fourier-based site amplification over four stiff soil sites for mainshock and aftershock of the 2001 Nisqually earthquake.

Table 3. Peak ground acceleration (PGA), frequency downshift in 1–2 Hz, amplitude-decrease factor in 3–4 Hz, and damping-increase factor in 1–2 and 3–4 Hz for soft and stiff soil sites. The numbers in parenthesis of SDS indicate that the damping-increase factors are calculated for the EW-component only, not the two horizontal components.

Sites	PGA of mainshock (g)		Freq.-downshift (Hz) (1–2 Hz)		Ampl.-reduction factor (3–4 Hz)		Damping-increase factor (HHT only)	
	NS	EW	HHT	Fourier	HHT	Fourier	(1–2 Hz)	(3–4 Hz)
Soft soil								
BOE	0.19	0.19	0.33	0.15	0.34	0.54	1.27	1.02
HAR	0.22	0.19	0.34	0.24	0.29	0.32	1.2	1.01
KDK	0.19	0.15	0.33	0.13	0.87	1.03	1.55	0.88
SDS	0.29	0.22	0.36	0.21	0.41	0.49	3.8 (1.84)	3.39 (1.75)
Average	0.22	0.19	0.34	0.18	0.48	0.60	1.96 (1.47)	1.57 (1.17)
(Average over BOE, HAR and KDK)							1.34	0.97
Stiff soil								
BHD	0.15	0.17	0.19	0.25	1.14	0.98	1.31	1.2
LAP	0.10	0.09	0.16	0.15	0.99	1.02	1.11	1.12
SEU	0.10	0.10	0.12	0.10	1.01	1.01	0.95	1.06
THO	0.09	0.12	0.18	0.15	0.75	1.04	0.7	1.03
Average	0.11	0.12	0.16	0.16	0.97	1.01	1.02	1.10
(Average over BHD, LAP and SEU)							1.12	1.13

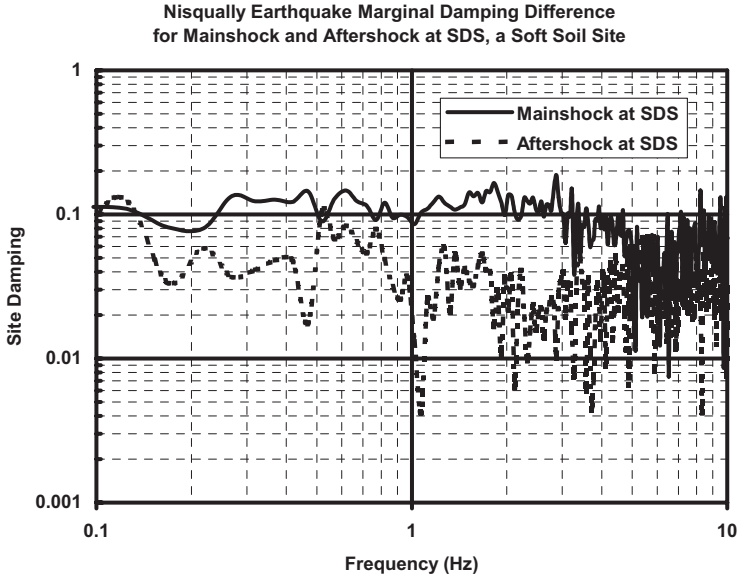

Fig. 19. Site damping at soft soil site SDS for mainshock and aftershock of the 2001 Nisqually earthquake.

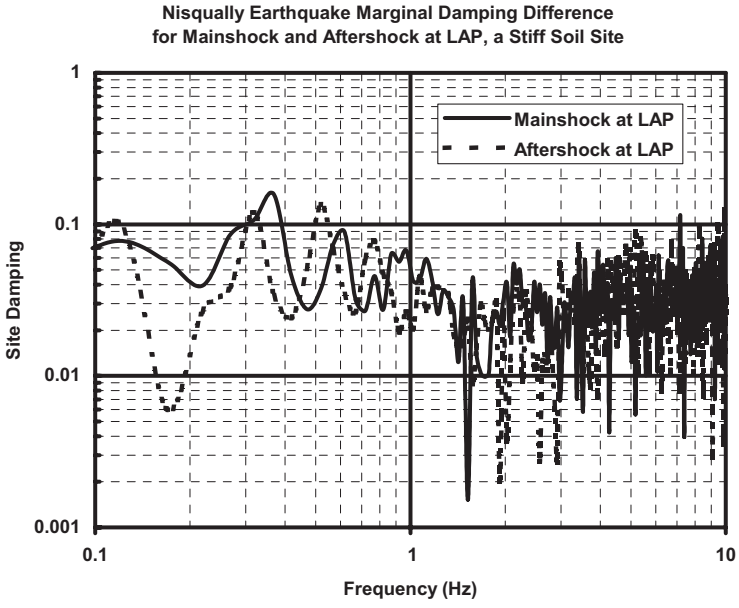

Fig. 20. Site damping at stiff soil site LAP for mainshock and aftershock of the 2001 Nisqually earthquake.

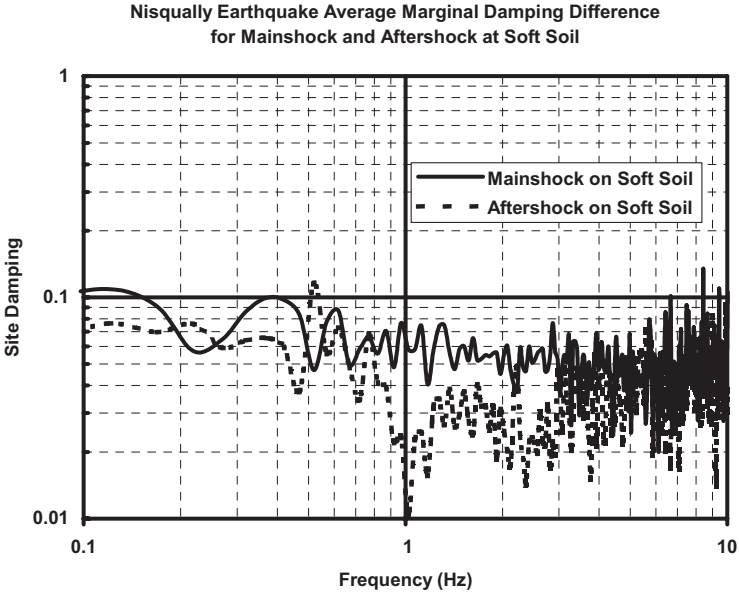

Fig. 21. Averaged site damping over four soft soil sites for mainshock and aftershock of the 2001 Nisqually earthquake.

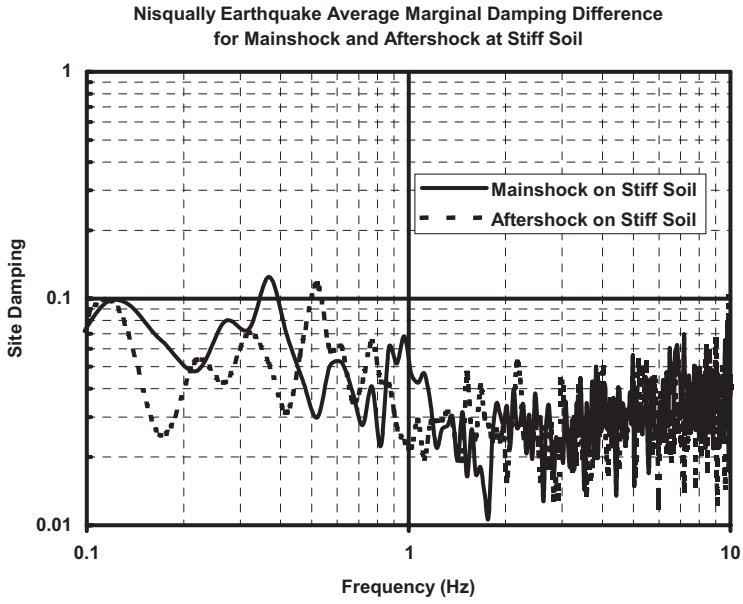

Fig. 22. Averaged site damping over four stiff soil sites for mainshock and aftershock of the 2001 Nisqually earthquake.

stronger site nonlinearity occurs during the mainshock at soft soil site than at the stiff soil site.

Figures 23 and 24 show the comparison of site damping at soft and stiff soil sites for aftershock and mainshock, respectively. Figure 23 displays almost the same site damping for the aftershock at both sites, while Fig. 24 shows the larger site damping at the soft soil site than at the stiff soil site. This suggests that the soft and stiff soil have the same damping nature or mechanism and the soft soil site for mainshock experiences larger site nonlinearity than the stiff soil site.

Since Fourier-based approach is not able to estimate appropriately the site damping, particularly for nonlinear sites, Table 3 only lists the damping-increase factors in two frequency bands that are calculated in a way similar to amplitude-reduction factor, i.e., the ratio of averaged damping of mainshock over a certain frequency band (i.e., 1–2 and 3–4 Hz) and that of aftershock.

As shown before, the HHT-based site damping is implicitly related to HHT-based site amplification. Therefore, the nonlinearity characterization and quantification from site amplification and damping should bear the relationship, if it is not completely explicit. It is likely difficult in practice to distinguish the influences of different nonlinearity characterization such as frequency downshift, amplitude-reduction factor from site amplification and damping-increase factor from site damping. Nevertheless, we next examine the relationship among the three nonlinearity indices from the limited data sets in Table 3.

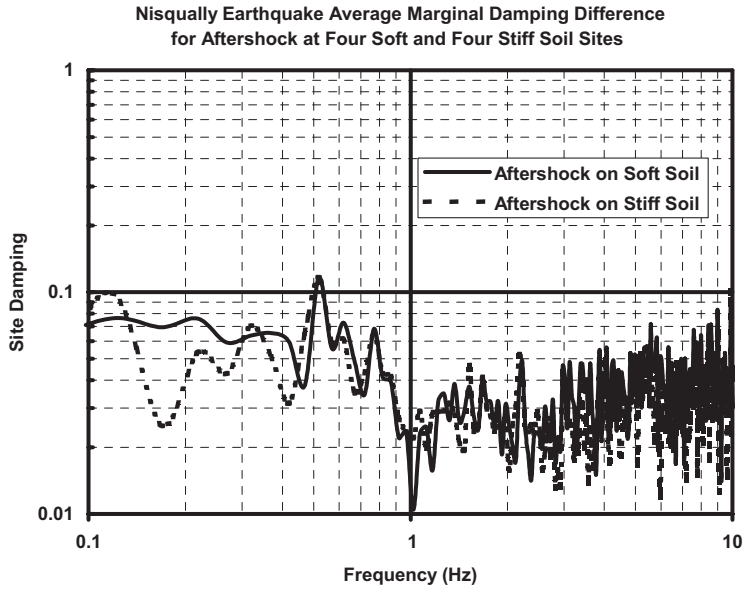

Fig. 23. Averaged site damping over four stiff and four soft soil sites for aftershock of the 2001 Nisqually earthquake.

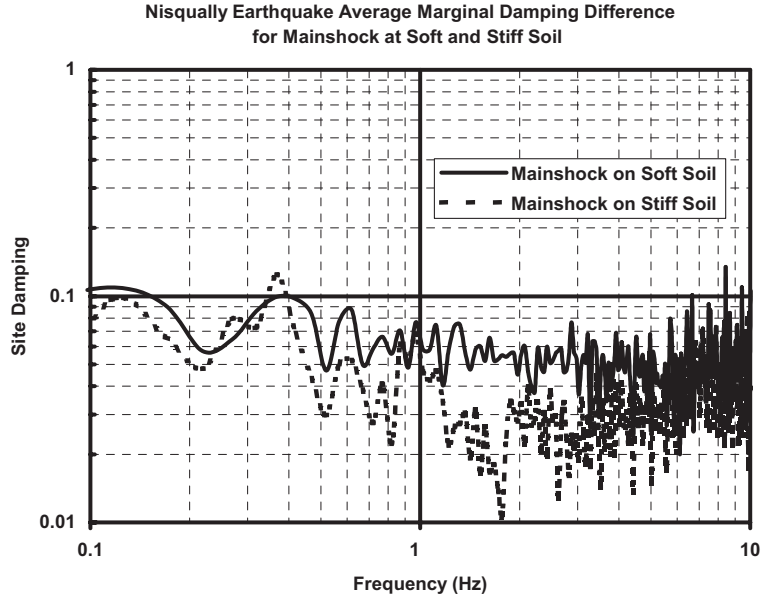

Fig. 24. Averaged site damping over four stiff and four soft soil sites for mainshock of the 2001 Nisqually earthquake.

Table 3 shows that the averaged damping-increase factors for stiff soil site are around unit (1) with 10% variation in both selected frequency bands (1–2 and 3–4 Hz), suggesting that the stiff soil site behaves linearly or weakly nonlinear during the mainshock from the perspective of damping change. This observation is basically consistent with that in terms of frequency downshift and amplitude-reduction factor in the site amplification. Note that the normalization of frequency downshift of 0.16 Hz for the stiff soil site to the center of the frequency band under investigation (i.e., 1.5 Hz of 1–2 Hz) is $10.7\% = 0.16/1.5$, which is marginally within 10% variation.

In contrast, Table 3 shows that the averaged damping-increase factors for the soft soil site are much larger than those in stiff soil site, implying that the soft soil site has strong nonlinear phenomena during the mainshock from the viewpoint of damping change. This fact agrees with the observations from frequency downshift and amplitude-reduction factors from the site amplification. In particular, the increased damping in 3–4 Hz for nonlinear soil will decrease ground motion, thus moderating the site amplification in the same frequency band. In the frequency band 1–2 Hz, the influences of site nonlinearity in the seismic ground motion may combine both effects of frequency downshift due to the loss of shear modulus and reduced amplitude of site-amplification factor due to the increased damping. Therefore, the large averaged frequency downshift of 0.34 for soft soil site is still compatible to the large averaged damping-increase factors of 1.96 in the frequency band of 1–2 Hz in characterizing the site nonlinearity.

Further examination of the damping-increased factors at each individual soft soil site suggests that the variation of the factors is large. In particular, the damping-increase factor at SDS is much larger than those at other sites. This phenomenon is not shown in the frequency downshift and amplitude-reduction factors for the same soft soil sites. This can be explained below.

All the soft soil sites except SDS have no liquefaction nearby. Recordings with liquefaction nearby will not only show the strong nonlinearity features in terms of frequency downshift and amplitude-reduction factors, it will also introduce abnormal, large-amplitude high-frequency spikes. Indeed, the abnormal spikes are observed explicitly in the NS-component of the recording at SDS in Fig. 14, but not in the EW-component of SDS and other recordings. To have a better understanding of influences of the abnormal spikes in the site damping, we compute the damping-increase factor at SDS in the EW direction only that is 1.84 Hz in 1–2 Hz and 1.75 Hz in 3–4 Hz shown in the parenthesis in Table 1, which are indeed much smaller than those calculated on the basis of two horizontal components of the recording at SDS. This suggests that the abnormal spikes significantly change the characterization of the damping at the site.

While the damping-increase factors in the EW direction at SDS are still larger than those at other sites, again attributable to the strong site nonlinearity with liquefaction nearby, they are comparable with others since the EW-component of recording at SDS shares the same motion features with others without abnormal

spikes. To this end, the NS-component of the recording at SDS can be regarded as a special recording with abnormal signals in this study. While that recording is useful in examining the features of liquefaction, it can be excluded for the statistical study here. To that end, Table 1 provides alternative averaged damping-increase factors with the factors at SDS calculated using two horizontal components replaced by those using the EW-component only. As a viable way, Table 3 also provides the averaged values over three sites excluding SDS. For comparison, the averaged damping-increase factors over three stiff soil sites are also supplied.

5. Concluding Remarks and Discussions

This study proposes an HHT-based approach in quantifying site nonlinearity for liquefaction diagnosis and nonlinear site amplification evaluation. In particular, it reveals the following:

1. Predominant instantaneous frequency of an earthquake motion is defined as the frequency with the largest amplitude in Hilbert amplitude spectra of the seismic recording at any time instant, and subsequently used together with other motion features for identifying site liquefaction conditions. Analysis of 29 sets of recordings at different liquefaction conditions shows that the proposed approach is more effective in detecting site liquefaction than other Fourier-based methods.
2. HHT-based site-amplification factor is defined as the ratio of marginal Hilbert amplitude spectra, similar to the Fourier-based one that is the ratio of Fourier amplitude spectra. The HHT-based factor has the following distinctive features in comparison with Fourier-based one.
   (i) The HHT-based factor is essentially equivalent to the Fourier-based one in quantifying linear or weakly-nonlinear site amplification and the changes of characteristics of weak nonlinearity.
   (ii) The HHT-based factor is more effective in quantifying site nonlinearity in terms of frequency downshift in the low-frequency range and amplitude-reduction factor with less oscillation in intermediate-frequency range than Fourier-based one.
   (iii) The HHT-based factor is generally larger than Fourier-based one in low-to-intermediate frequency range for strong site nonlinearity.
3. Instantaneous damping, and Hilbert and marginal Hilbert damping spectra are defined in ways similar to instantaneous frequency, and Hilbert and marginal Hilbert amplitude spectra, respectively. Consequently, the HHT-based site damping is found as the difference of marginal Hilbert damping spectra, which can be used as an alternative index to measure the influences of site nonlinearity in seismic ground responses.

Seismic damage to structures takes the form of amplified crack and defects, partial loss of resisting moment in the connections, the formation of plastic hinges in piles, etc., which can be effectively characterized with structural nonlinearity in terms of

stiffness reduction, damping increase, and dynamic amplification reduction. Therefore, the proposed approach in this study can be in principle used to quantify the structural nonlinearity from seismic response recordings in structures, which could play a key role in accurately assessing seismic damage to structures, and ultimately aid in mitigating seismic hazard to structural systems.

Acknowledgments

The author would like to express his sincere gratitude to Norden E. Huang at NASA, Stephen Hartzell, Authur Frankel, and Erdal Safak at USGS, Lance VanDemark from Colorado School of Mines, and Yuxian Hu from China Seismological Bureau and Jianwen Liang from Tianjin University in China for providing data, Fourier analysis and results, and more important, constructive suggestions. This work was supported by the National Science Foundation with Grant Nos. 0085272 and 0414363, and by US-PRC Researcher Exchange Program administered by Multidisciplinary Center for Earthquake Engineering Research. The opinions, findings, and conclusions expressed herein are those of the author and do not necessarily reflect the views of the sponsors.

References

1. NEHRP (National Earthquake Hazards Reduction Program) recommended provisions for seismic regulations for new buildings (1997). Federal Emergency Management Agency Report FEMA 302, Washington DC, p. 337.
2. A. Frankel, C. Mueller, T. Barnhard, D. Perkins, E. Leyendecker, N. Dickman, S. Hanson and M. Hopper, USGS national seismic hazard maps, *Earthquake Spectra* **16** (2000) 1–19.
3. D. Bernal and J. L. Beck, Special issue on phase I of the IASC-ASCE structural health monitoring benchmark, *J. Eng. Mech. ASCE* **130**(1) (2004) 1–104.
4. N. E. Huang, S. Zheng, S. R. Long, M. C. Wu, H. H. Shih, Q. Zheng, N.-C. Yen, C. C. Tung and M. H. Liu, The empirical mode decomposition and Hilbert spectrum for nonlinear and nonstationary time series analysis, *Proc. Roy. Soc. Lond. A* **454** (1998) 903–995.
5. K. Worden and G. R. Tomlinson, *Nonlinearity in Structural Dynamics — Detection, Identification and Modeling* (Institute of Physics Publishing, Bristol and Philadelphia, 2001).
6. R. Zhang, L. VanDemark, J. Liang and Y. X. Hu, On estimating site damping with soil nonlinearity from earthquake recordings, *Int. J. Non-Linear Mech.* **39** (2004) 1501–1517.
7. R. Zhang, S. Hartzell, J. Liang and Y. X. Hu, An alternative approach to characterize nonlinear site effects, *Earthquake Spectra* **21** (2005) 243–274.
8. N. E. Huang, M. L. Wu, S. R. Long, S. P. Shen, W. Wu, P. Gloersen and K. L. Fan, A confidence limit for the empirical mode decomposition and Hilbert spectral analysis, *Proc. Roy. Soc. Lond. A* **459** (2003) 2317–2345.
9. S. L. Kramer, *Geotechnical Earthquake Engineering* (Prentice-Hall, Inc. Upper Saddle River, NJ, 1996).
10. T. L. Youd, I. M. Idriss, R. D. Andrus, I. Arango, G. Castro, J. T. Christian, R. Dobry, W. D. L. Finn, L. F. Harder Jr., M. E. Hynes, K. Ishihara, J. P. Koester,

S. S. C. Liao, W. F. Marcuson III, G. R. Martin, J. K. Mitchell, Y. Moriwaki, M. S. Power, P. K. Robertson, R. B. Seed and K. H. Stokoe II, Liquefaction resistance of soils: Summary report from the 1996 NCEER and 1998 NCEER/NSF Workshops on evaluation of liquefaction resistance of soil, *ASCE J. Geotech. Geoenviron. Eng.* **127** (2001) 817–833.

11. T. L. Youd, J. P. Bardet and J. D. Bray, Kocaeli, Turkey, Earthquake of August 17, 1999 Reconnaissance Report, *Earthquake Spectra* **16** (Supp A) (2000) 1–456.
12. J. Uzarski and C. Arnold, Chi-Chi, Taiwan, Earthquake of September 21, 1999 Reconnaissance Report, *Earthquake Spectra* **17** (Supp A) (2001) 1–183.
13. T. Suzuki, Y. Shimizu and W. Nakayama, Characteristics of strong motion records at the liquefied sites and judgment for liquefaction, in *11th European Conference on Earthquake Engineering*, Paris, France, 6–11 September, 1998, CD-ROM. Balkema: Rotterdam.
14. M. V. Kostadinov and F. Yamazaki, Detection of soil liquefaction from strong motion records, *Earthquake Eng. Struct. Dynam.* **30** (2001) 173–193.
15. M. J. Bennett, P. V. McLaughlin, J. S. Sarmiento and T. L. Youd, Geotechnical investigation of liquefaction site, Imperial Valley, California, Open-file Rep. 84-252, 1984, U.S. Geological Survey, Washington, D.C.
16. T. L. Youd, Physics and Mechanics of Liquefaction from fields records and experience, in *Phys. Mech. Soil Liquefact.*, eds. Lade and Yamamuro (Balkema, Rotterdam, 1999), pp. 325–334.
17. C. Y. Chang, C. M. Mok, M. S. Power and Y. K. Tang, Analysis of ground response data at lotung large-scale soil-structure interaction experiment site, Rep. No. NP-7306-SL (1991), Electric Power Research Institute, Palo Alto, Calif.
18. Y. X. Hu, S. C. Liu and W. M. Dong, *Earthquake Engineering* (Champman & Hall, London, 1996).
19. R. D. Borcherdt, Empirical evidence for site coefficients in building code provisions, *Earthquake Spectra* **18** (2002) 189–217.
20. S. Hartzell, Variability in nonlinear sediment response during the 1994 Northridge, California, earthquake, *Bull. Seism. Soc. Am.* **88** (1998) 1426–1437.
21. D. R. H. O'Connell, Influence of random-correlated crustal velocity fluctuations on the scaling and dispersion of near-source peak ground motions, *Science* **283** (1999) 2045–2050.
22. N. Yoshida and S. Iai, Nonlinear site response and its evaluation and prediction, *The Effects of Surface Geology on Seismic Motion*, eds. Irikura, Kudo, Okada and Sasatani (Balkema, Rotterdam, 1998), pp. 71–90.
23. R. Zhang, S. Ma, E. Safak and S. Hartzell, Hilbert–Huang transform analysis of dynamic and earthquake motion recordings, *ASCE J. Eng. Mech.* **129**(8) (2003) 861–875.
24. A. D. Frankel, D. L. Carver and R. A. Williams, Nonlinear and linear site response and basin effects in Seattle for the M6.8 Nisqually, Washington, Earthquake, *Bull. Seism. Soc. Am.* **92** (2002) 2090–2109.